DOI: 10.1002/cssc.201301152

Role of Ultrathin Metal Fluoride Layer in Organic Photovoltaic Cells: Mechanism of Efficiency and Lifetime Enhancement

Kyung-Geun Lim,[a] Mi-Ri Choi,[a] Ji-Hoon Kim,[b] Dong Hun Kim,[a] Gwan Ho Jung,[a] Yongsup Park,*[b] Jong-Lam Lee,[a] and Tae-Woo Lee*[a]

Although rapid progress has been made recently in bulk heterojunction organic solar cells, systematic studies on an ultrathin interfacial layer at the electron extraction contact have not been conducted in detail, which is important to improve both the device efficiency and the lifetime. We find that an ultrathin BaF_2 layer at the electron extraction contact strongly influences the open-circuit voltage (V_{oc}) as the nanomorphology evolves with increasing BaF_2 thickness. A vacuum-deposited ultrathin BaF_2 layer grows by island growth, so BaF_2 layers with a nominal thickness less than that of single-coverage layer ($\approx$3 nm) partially cover the polymeric photoactive layer. As the nominal thickness of the BaF_2 layer increased to that of a single-coverage layer, the V_{oc} and power conversion efficiency (PCE) of the organic photovoltaic cells (OPVs) increased but the short-circuit current remained almost constant. The fill factor and the PCE decreased abruptly as the thickness of the BaF_2 layer exceeded that of a single-coverage layer, which was ascribed to the insulating nature of BaF_2. We find the major cause of the increased V_{oc} observed in these devices is the lowered work function of the cathode caused by the reaction and release of Ba from thin BaF_2 films upon deposition of Al. The OPV device with the BaF_2 layer showed a slightly improved maximum PCE (4.0%) and a greatly (approximately nine times) increased device half-life under continuous simulated solar irradiation at 100 mW cm^{-2} as compared with the OPV without an interfacial layer (PCE = 2.1%). We found that the photodegradation of the photoactive layer was not a major cause of the OPV degradation. The hugely improved lifetime with cathode interface modification suggests a significant role of the cathode interfacial layer that can help to prolong device lifetimes.

Introduction

As a result of their flexibility and low cost, organic photovoltaic cells (OPVs) are promising candidates for the next generation of solar cells.[1–3] Although the power conversion efficiency (PCE) of OPVs has been greatly improved recently,[4,5] a systematic study is required to clarify the phenomenon of charge extraction, which strongly affects device efficiency and lifetime. In bulk heterojunction OPVs, charge extraction from the photoactive layer to each electrode is affected critically by the interface of the photoactive layer with electrodes.[3] To obtain efficient electron extraction, materials of many types have been employed as the interlayer of the cathode.[6–10] Alkali and alkali earth metals (e.g., Mg, Ca, Ba) have been used as the interfacial cathode layer and have a great influence on the open-circuit voltage (V_{oc}).[3] The work function (WF) of the electrodes is mainly responsible for the built-in electric field in the charge-extraction pathway.

However, the WFs of alkali and alkali earth metals are closer to the vacuum level than those of nonreactive high-WF metals (e.g., Al, Ag, Au) so that they are prone to react with oxygen and moisture. To prevent reactive metals from oxidizing into nonconducting metal oxides, a thin layer of metal fluoride (e.g., LiF, CaF_2, CsF) can be used as the cathode interlayer instead of pure reactive metals with a low WF.[8–10]

Although these metal fluoride interfacial layers are insulators, they help transport photogenerated electrons efficiently to the cathode; this phenomenon has been explained by three different models. The reaction model suggests that the deposition of a reactive Al metal on LiF, CaF_2, or CsF induces a chemical reaction of Al with the metal fluorides and then releases low-WF atoms (i.e., Li, Ca, Cs), which leads to the effective extraction of photogenerated electrons by tuning the effective WF.[9] The dipole model suggests the large dipole moment of metal fluorides (e.g., 6.33 D for LiF) decreases the effective WF of the negative electrode by decreasing the surface potential of the Al.[11] The tunneling model suggests that electron transport through the metal fluoride interlayer increases as a result of the decrease of the effective barrier caused by the reduced band bending of the active layer if the insulating interfacial layer is thin enough to permit effective electron tunneling.[7] The validity of these models is under debate in OPVs as well as

[a] K.-G. Lim, M.-R. Choi, D. H. Kim, G. H. Jung, Prof. J.-L. Lee, Prof. T.-W. Lee
Department of Materials Science and Engineering
Pohang University of Science and Technology (POSTECH)
San 31 Hyoja-dong, Nam-gu, Pohang, Gyungbuk 790-784 (Korea)
E-mail: twlee@postech.ac.kr

[b] J.-H. Kim, Prof. Y. Park
Department of Physics and Research Institute for Basic Sciences
Kyung Hee University
Seoul 130-701 (Korea)
E-mail: parky@khu.ac.kr

Supporting Information for this article is available on the WWW under http://dx.doi.org/10.1002/cssc.201301152.

organic light-emitting diodes (OLEDs). Therefore, the clarification of the role of metal fluorides in OPVs is needed. In this work, we employed a BaF_2 interfacial layer instead of the conventional LiF layer and then investigated the roles of the BaF_2 layer on the PCE, V_{oc}, fill factor (FF), short-circuit current (J_{sc}), and lifetime of the devices. Morphological changes of the metal fluoride interfacial layers with increasing thickness explain their great influence on device efficiency and lifetime. We used a combinatorial thermal evaporator to fabricate devices with various BaF_2 thicknesses after loading all samples to the vacuum chamber together, which helps to exclude the plausible batch-to-batch variation of the performance observed in solution-processed polymer photovoltaic devices. The V_{oc} and PCE increased as the nominal thickness of the BaF_2 layer increased to the thickness of a single-coverage layer (≈3 nm), whereas the FF and PCE decreased significantly as the nominal thickness increased further. We discuss the electron extraction mechanism in OPVs that have BaF_2 interfacial layers. The optimum PCE was higher in a device with a BaF_2 interfacial layer (4.0%) than in one with a LiF layer (3.8%). We also demonstrate that devices with a BaF_2 interfacial layer had significantly increased lifetimes under continuous simulated solar irradiation. We show clearly that the higher performance, especially V_{oc}, observed in devices with a metal fluoride layer of less than a single-coverage-layer thickness is because of the lowered WF caused by the reaction of BaF_2 and the release of pure metal (Ba) upon the deposition of reactive Al on the metal fluoride film (BaF_2). Some BaF_2 dissociated into Ba and F and thus allowed the formation of AlF_3 upon deposition of reactive Al; these reactions were a major cause of the lowered WF if the insulating layer of unreacted BaF_2 and newly formed AlF_3 was thin enough for the electrons to tunnel through.

Results and Discussion

We fabricated OPVs by using a poly(3-hexylthiophene) (P3HT):[6,6]-phenyl-C_{61}-butyric acid methyl ester (PCBM) blend as a photoactive layer, poly(3,4-ethylenedioxythiophene): poly(4-styrenesulfonate) (PEDOT:PSS) as a hole-extraction layer, and BaF_2 as an electron extraction interfacial layer. In polymer solar cells based on the semicrystalline donor polymer P3HT, the device PCE tends to be sensitive to the film preparation conditions (e.g., drying and thermal annealing conditions), which, in turn, influence the chain morphology compared with devices that use amorphous photoactive polymers.[12,13] To study the effect of ultrathin interfacial layers of various thickness on the OPV PCE, all the samples should ideally be fabricated and characterized at the same time to avoid possible batch-to-batch variation of experimental conditions during preparation steps. Therefore, we fabricated all of the samples at the same time by using a combinatorial thermal evaporator instead of fabricating them separately by using a general thermal evaporator. The combinatorial chamber allows the systematical change in the thickness of the BaF_2 interfacial layers of the negative electrodes in OPVs without breaking the chamber vacuum after loading the samples.

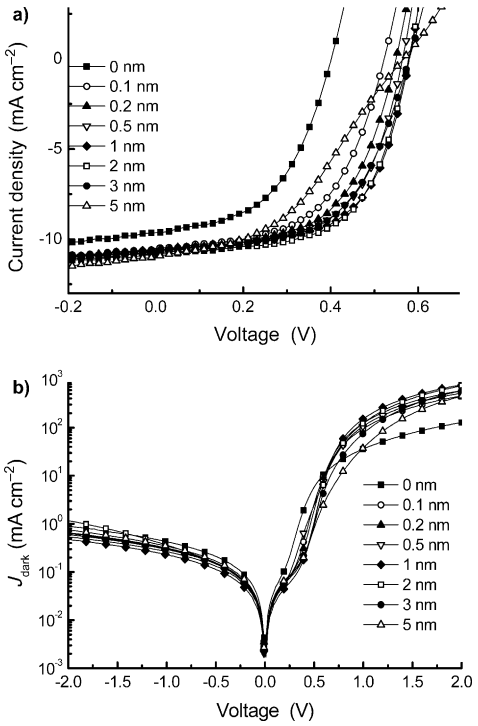

Figure 1. *J–V* characteristics of the OPV devices with various BaF_2 thicknesses a) under simulated solar AM 1.5G illumination at an intensity of 100 mW cm^{-2} and b) under dark conditions.

We measured the current density–voltage (*J–V*) characteristics in OPV devices with various thicknesses of BaF_2 interfacial layers (0, 0.1, 0.2, 0.5, 1, 2, 3, and 5 nm) under air mass 1.5 G solar simulated light irradiation of 100 mW cm^{-2} (Figure 1 a) and under dark conditions (Figure 1 b). The J_{sc}, V_{oc}, FF, and PCE values of the devices varied with BaF_2 thickness (Table 1). The reference device without a BaF_2 interfacial layer had V_{oc} = 0.40 V. The V_{oc} increased significantly (to 0.51 V) even in the device with a nominal 0.1 nm thick BaF_2 layer. The V_{oc} seemed

Table 1. V_{oc}, J_{sc}, FF, R_{sh}, R_s, and PCE of the polymer photovoltaic cells with various interlayers.

Interlayer	V_{oc} [V]	J_{sc} [mA cm^{-2}]	FF [%]	R_{sh} [Ω cm^2]	R_s [Ω cm^2]	PCE [%]
Al only[a]	0.400	10.0	53.1	253.8	10.8	2.1
BaF_2 0.1 nm[a]	0.511	10.5	57.1	486.6	10.1	3.1
BaF_2 0.2 nm[a]	0.538	10.6	57.6	570.6	7.7	3.4
BaF_2 0.5 nm[a]	0.552	10.6	58.1	639.0	6.7	3.4
BaF_2 1 nm[a]	0.565	10.6	61.4	508.8	7.4	3.7
BaF_2 2 nm[a]	0.566	10.8	61.5	516.0	8.2	3.8
BaF_2 3 nm[a]	0.572	10.8	57.6	551.4	11.7	3.6
BaF_2 5 nm[a]	0.565	10.9	42.2	384.6	30.9	2.6
LiF 1 nm[b]	0.540	10.4	65.1	923.4	5.9	3.8
Ba 1 nm[b]	0.556	10.6	66.0	622.8	5.3	4.0
BaF_2 1 nm[b]	0.560	10.7	65.3	535.2	5.7	4.0

[a] P3HT:PCBM films were dried promptly in a circulating N_2-filled glovebox for ≈3 min after spin casting to reduce the time deviation of device processing. [b] P3HT:PCBM films were slowly dried in a N_2-filled glovebox for ≈12 min to maximize the PCE as a result of a slow drying effect.

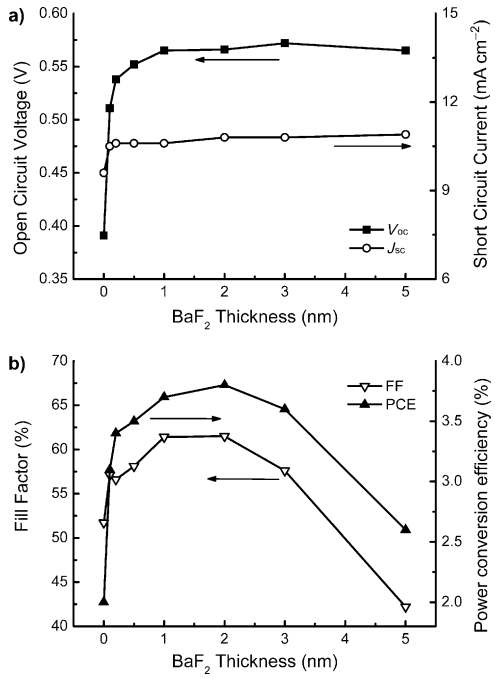

Figure 2. Variation of the device performance parameters with BaF_2 thickness: a) V_{oc} and J_{sc} and b) PCE and FF.

to saturate above a 1 nm thickness (Figure 2a). The strong dependence of V_{oc} on the BaF_2 thickness implies that the built-in potentials (V_{bi}) of the devices increase with increasing thickness; this effect will be discussed later. All the device performance parameters, such as V_{oc}, J_{sc}, and PCE, were almost identical for devices with 1–3 nm BaF_2 layers (Table 1). The maximum device performance ($V_{oc}=0.57$ V, $J_{sc}=10.8$ mA cm^{-2}, PCE = 3.8%) was obtained with a 2 nm BaF_2 layer. As the BaF_2 thickness increased up to <3 nm, the series resistance (R_s) tended to decrease, the shunt resistance (R_{sh}) tended to increase, and thus the FF tended to increase (Table 1). The PCE decreased as the BaF_2 thickness increased beyond 3 nm because of the reduced FF (Table 1 and Figure 2b). A BaF_2 layer thicker than a single-coverage layer is an insulator and forms a barrier to electron tunneling. BaF_2 deposited on the polymer film had a thickness of a single-coverage layer at 3 nm (Figure 3).[14] In OLEDs that operate at voltages higher than the V_{bi} of a typical OPV, the device luminous efficiencies did not degrade meaningfully even with much thicker metal fluoride layers (e.g., 8 nm).[15] However, in OPVs operated with a much smaller V_{bi} than the operating voltages of OLEDs, the tunneling barrier is difficult to overcome if the metal fluoride layer is thicker than a single-coverage layer. Although the V_{oc} was still high in the device with a BaF_2 layer thicker than a single-coverage layer, the insulating nature of BaF_2 and electron accumulation at the interface because of the blockage of extraction increased the R_s from 11.7 Ω cm^2 at 3 nm to 30.9 Ω cm^2 for a 5 nm BaF_2 interfacial layer and thus reduced the FF, which caused the S-shaped *J–V* behavior in the device with a 5 nm thickness (Figure 1a).

BaF_2 follows the island-growth mode on the polymer surface under vacuum deposition conditions (Figure 3a); this mode is

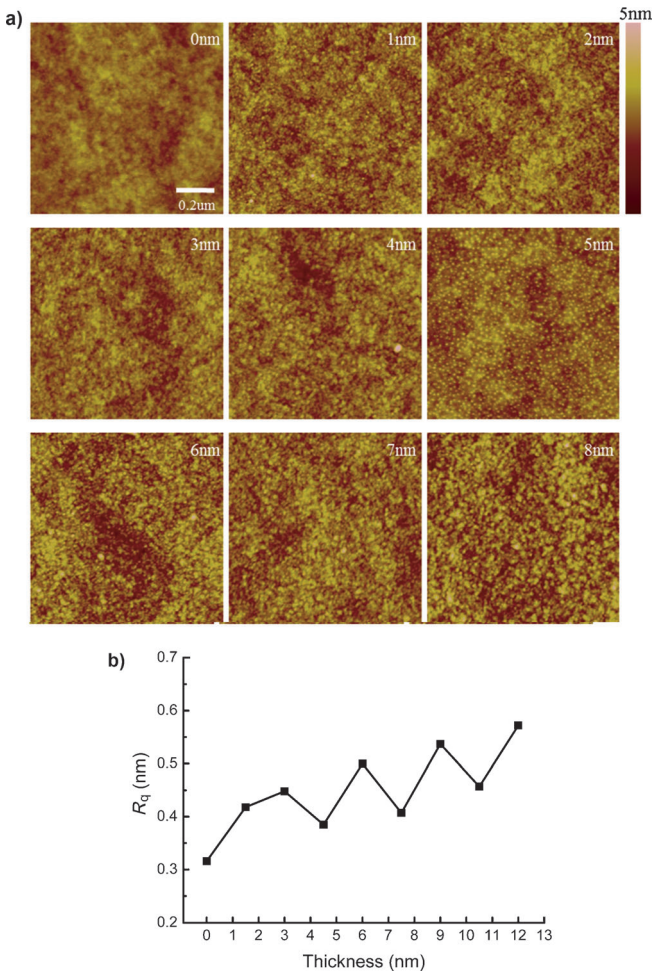

Figure 3. a) AFM images of thermally evaporated BaF_2 on the polymer surface with varying thickness. b) Average RMS of roughness (R_q) versus BaF_2 thickness.

similar to the growth of LiF.[14,16] The grain size of BaF_2 tended to increase as the deposited nominal thickness increased as monitored by using a quartz crystal microbalance sensor. The average root-mean-square (RMS) roughness also increased as the BaF_2 thickness increased from 0.333 (pristine polymer surface) to 0.436 nm (3 nm BaF_2) because the BaF_2 grain grows to the larger island to form a single-coverage layer.

If additional BaF_2 was deposited on the surface, small BaF_2 grains started to grow on top of one layer and thus the space between the large grains was filled by these, and the RMS roughness decreased to 0.369 nm (4.5 nm BaF_2). Therefore, the first RMS roughness peak can be found at the thickness of a single-coverage layer ($\approx$3 nm; Figures 3b and S1). Once the recessed regions between the large grains were filled by small BaF_2 grains, they tended to grow further and thus the RMS roughness increased again to 0.508 nm (6 nm BaF_2). This repeated growth and filling process of BaF_2 grains was well presented in the AFM data (Figure 3b). If the BaF_2 layer is thinner than a single-coverage layer, different electron extraction paths are possible, through BaF_2 islands or directly to the Al electrode (Figure 4a). The nanomorphology evolution of the BaF_2 islands before single-coverage-layer formation strongly affect-

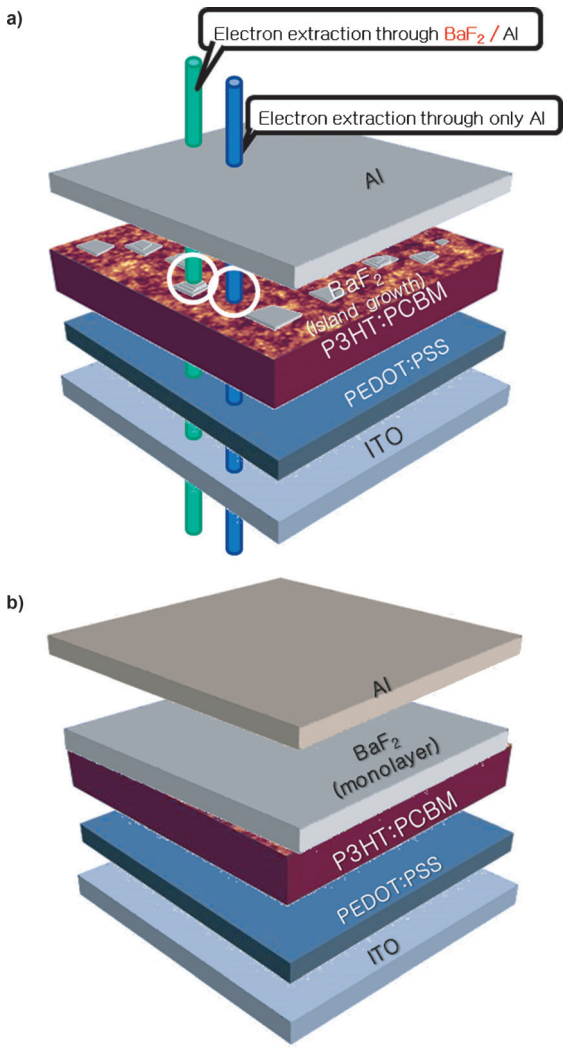

Figure 4. Schematic device configurations of P3HT:PCBM solar cells. a) Island-growth mode of a BaF_2 interfacial layer on a P3HT:PCBM photoactive layer. If the nominal thickness of the BaF_2 layer is less than that of a single-coverage layer ($< \approx 3$ nm), two different charge-extraction paths coexist because of the existence of BaF_2 islands that do not fully cover the photoactive layer. b) If the BaF_2 thickness is thicker ($> \approx 3$ nm) than a single-coverage layer, the BaF_2 layer covers most of the photoactive layer surface so that the electrons must pass through the insulating interlayer to be extracted to the cathode.

ed the decrease of the cathode WF up to a certain point of metal fluoride coverage (or nominal thickness); this effect resulted in gradual increases of V_{bi} and thus V_{oc} of the devices as a function of nominal thickness (Figures 2a and S1 f).

This V_{oc} improvement can be explained by the decreased effective WF of the negative electrode (Al) because the BaF_2 layer induces a shift in the surface WF according to the reaction model or the dipole model. Such a reduction has been observed previously in polymer light-emitting diodes that use a thin metal fluoride layer by electroabsorption measurements that estimate the V_{bi} of the devices based on the Schottky–Mott model and an approximation of the rigid tilting of polymer energy levels with bias.[16] Based on the bulk chemical reaction of BaF_2 with the reactive Al metal shown in Equation (1), the overall heat of formation is 605.44 kJ mol^{-1}, indicative of an endothermic reaction.[14]

$$3\,BaF_2 + 2\,Al \rightarrow 3\,Ba + 2\,AlF_3 \quad (1)$$

Additional thermal energy required for the exchange reaction can be provided by the latent heat released by evaporated Al atoms upon deposition.[14] The effective WF of the BaF_2/Al cathode estimated by a photovoltaic measurement[17] was 2.9 eV (with thicker BaF_2 than a single-coverage layer), whereas the Ba WF is 2.7 eV.[14] However, the exchange reaction occurs dominantly on the surface of BaF_2; therefore, if the BaF_2 layer is thicker than the depth to which Al atoms penetrate the BaF_2 layer, unreacted BaF_2 still acts as a dipole layer. From classical electrostatics, the dipole layer near the electrode causes a decrease ($\Delta\Phi$) in the energy barrier at the interface given by Equation (2):

$$\Delta\Phi = N\mu/\varepsilon_0\varepsilon \quad (2)$$

in which N is the number of charges per unit surface, μ is the dipole moment, ε_0 is the vacuum permittivity, and ε is the static dielectric constant.[18,19] Therefore, the decreased effective WF of the BaF_2/Al electrode can result from dipole-layer formation at the interface or from the combined contribution of dipole-layer formation and the low-WF metal released by reaction; the dipole moments of unreacted BaF_2, the low WF of the Ba released upon Al deposition, and dipole moments of the reaction product AlF_3 eventually leads to an increase of V_{bi} and thus of V_{oc}.

To elucidate the effect of the BaF_2 layer on the OPV performance, BaF_2/Al and Ba/Al electrodes were compared. A Ba interfacial layer also produced a gradual increase of the V_{oc}, which was also correlated to the island-growth mode of Ba similar to the growth mode of BaF_2 (Figure 5). The V_{oc} values of OPVs with a Ba/Al electrode were also almost saturated above 1 nm thickness, similar to those with the BaF_2/Al electrode. Once the surface was covered by Ba to a thickness greater than a single-coverage layer (≈ 3 nm as determined from the AFM images shown in Figure S2), no further changes in WF and thus V_{oc} occurred (Figure 5). The common phenomenon that V_{oc} is a function of the nominal thickness of both the Ba and BaF_2 interfacial layers suggests that the change in V_{oc} is a consequence of the morphological evolution of the layer during island growth. However, because Ba is metallic, unlike BaF_2, the device with a 5 nm thick Ba layer maintained the saturated FF, J_{sc}, and PCE, unlike the device with a 5 nm thick BaF_2 layer (Table 1). This result supports the idea that the poor PCE of OPVs with BaF_2 thicker than a single-coverage layer can be ascribed to the insulating nature of the thick BaF_2 that impedes charge transfer across the interface.

We also investigated the effect of an ultrathin BaF_2 interfacial layer by measuring the capacitance–voltage (C–V) characteristics at 1000 Hz. In general, the capacitance tended to increase to a peak as a function of the applied voltage and then decreased immediately. The capacitance is mainly correlated with the accumulated space charges inside the devices. The

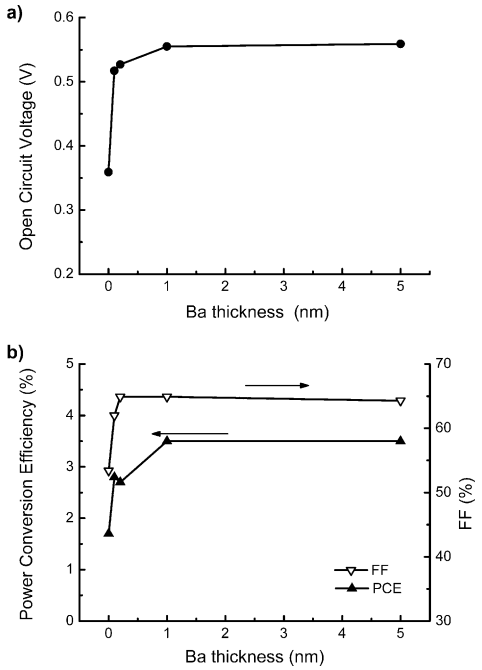

Figure 5. Device performance of P3HT:PCBM solar cells that have a Ba cathode interlayer as a function of Ba thickness: a) V_{oc} and b) PCE and FF.

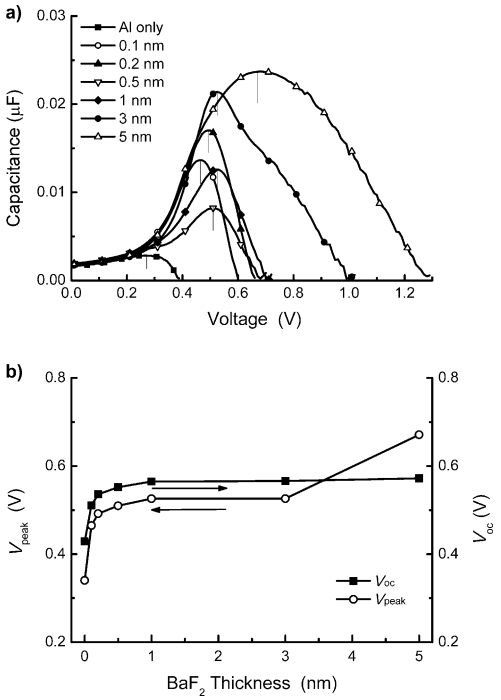

Figure 6. a) *C–V* characteristics of P3HT:PCBM solar cells versus the thickness of BaF_2 interfacial layers. Vertical lines: peak points. b) V_{peak} and V_{oc} versus BaF_2 thickness.

distinct capacitance peaks changed consistently as a function of BaF_2 thickness. The voltage at the peak capacitance (V_{peak}) is correlated with V_{bi} according to Equation (3):[20]

$$V_{bi} - V_{peak} \propto \frac{k_B T}{e} \quad (3)$$

in which k_B is the Boltzman constant, T is the absolute temperature, and e is the magnitude of the electron charge. The V_{peak} value is always smaller than V_{bi} at room temperature because of the space charges near the electrodes, and V_{peak} approaches V_{bi} as the temperature decreases. Therefore, at room temperature, V_{peak} is considered to be an effective value of V_{bi}. In OPVs, a high V_{peak} implies a high V_{bi} (Figure 6b). V_{peak} as a function of thickness has the same trend as V_{oc} (Figure 6b), which implies that V_{peak} at room temperature was observed at the open-circuit condition (or flat-band condition). At voltages above the open-circuit condition, the capacitance tended to decrease sharply because of the recombination of space charges with injected opposite charges. However, the correlation of V_{peak} with V_{bi} above 3 nm BaF_2 interfacial thickness (e.g., 5 nm) deviated from the trend observed below 3 nm thickness. The capacitance at higher voltages than V_{peak} in the device with 5 nm BaF_2 tended to decay more slowly than in devices with thinner layers; this tendency implies that the accumulated charges near the thick BaF_2 layer were not dissipated effectively by recombination with injected charge carriers.

We performed X-ray photoelectron spectroscopy (XPS) of the Al 2p and F 1s peaks for Al deposited up to 1.5 nm on a 3.0 nm BaF_2 film surface (Figure 7). The Al 2p core-level spectrum (Figure 7a) of 3.0 nm of BaF_2 on the P3HT:PCBM layer before Al was deposited showed no Al 2p feature as expected. If 0.5 nm of Al was deposited, a single peak (Al1) at 76.24 eV was obtained by using a peak-fitting routine as indicated by the colored peaks shown in Figure 7b. After 1.0 nm of Al was deposited, this peak shifted to 76.01 eV and two additional peaks emerged at lower binding energies of 73.32 (Al2) and 74.56 eV (Al3) after detailed peak fitting (Figure 7c). This appearance of the new peaks indicates that new chemical states of Al were formed; the nature of the new chemical states will be discussed later. Further deposition of Al up to 2.0 nm shifted the binding energies of the peaks to 75.87, 74.50, and 73.18 eV for the Al1, Al2, and Al3 peaks, respectively. The intensities of the Al2 and Al3 peaks (i.e., new chemical states) in-

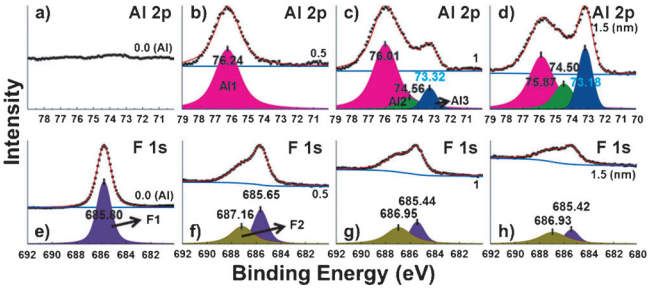

Figure 7. a) Al 2p XPS spectra for 3.0 nm of BaF_2 on a P3HT:PCBM layer. b)–d) Evolution of the Al 2p peak with increasing Al thickness on the BaF_2 layer. e) F 1s XPS spectra for 3.0 nm of BaF_2 on a P3HT:PCBM layer. f)–h) Similar F 1s XPS spectra. Dots: measured data; red lines: results of least-square peak-fitting procedures by using Voigt function peak shapes; colored peaks: fitting components. F1 and F2 indicate the F 1s core-level peaks from BaF_2 and AlF_3, respectively.

creased significantly with the increasing amount of Al deposition (Figure 7c and d). The intensity ratio (Al1/Al2/Al3) changed from 1.00:0.18:0.33 at 0.5 nm of Al to 1.00:0.48:1.16 at 1.5 nm of Al, which was deposited by using effusion cells at the rate of approximately 1 nm min^{-1}.

The F 1s core-level XPS spectrum obtained for a pristine 3.0 nm BaF_2 film surface showed only a single F 1s peak (F1) at 685.80 eV (Figure 7e). Clearly, this peak is because of the F atoms in the BaF_2 film. After 0.5 nm of Al deposition, the original F 1s peak moved to 685.65 eV and an additional peak (F2) appeared at a higher binding energy of 687.16 eV (Figure 7f). After 1.0 (Figure 7g) and 1.5 nm (Figure 7h) of Al deposition, a new chemical state of fluorine, which is different from the fluorine atom in BaF_2, appeared. The intensity ratio (F1/F2) of the two F 1s peaks was 1.00:1.92 for 0.5 nm of Al (Figure 7f), which changed to 1.00:1.32 at 1.0 nm of Al and 1.00:1.20 at 1.5 nm of Al.

Reference spectra[24,25] indicate that the Al1 peak (76.01 eV, Figure 7) is caused by Al atoms in Al–F bonds, Al2 (74.56 eV) is a result of Al–O, and Al3 (73.32 eV) is because of metallic Al. Similarly, for 0.5 nm of Al deposition, F1 (685.65 eV) is a result of BaF_2 and F2 (687.16 eV) is caused by AlF_3. These peak identifications indicate clearly that Al atoms adsorbed on the BaF_2 film break Ba–F bonds and make Al–F bonds to form a thin layer of AlF_3 on BaF_2 and that at 0.5 nm of Al most of the deposited Al atoms form AlF_3 as evidenced by the single Al 2p peak (Figure 7b). However, the intensity ratio of the F 1*s* peak from BaF_2 and AlF_3 did not change much at 1.0 and 2.0 nm of Al deposition; thus the AlF_3 thickness did not increase with increasing Al deposition; that is, the AlF_3 layer is more or less confined to the near-surface region of the BaF_2 film. This conclusion is consistent with the evolution of Al 2p peaks, in which the Al 2p peak from AlF_3 slowly decreased with increasing Al deposition, whereas the Al oxide and metallic Al peaks naturally increased. As a reaction between Al and BaF_2 occurred, released metallic Ba and the resultant formation of AlF_3 upon reaction seem to be primary factors for the change in WF. Therefore, we conclude that if a BaF_2 layer thinner than a single-coverage layer was deposited on the polymer layer in OPVs, the increased V_{oc} can be understood primarily by this reaction model.

We further optimized the device performance by controlling the conditions under which a spin-cast P3HT:PCBM layer was dried (Table 1) and compared the performance of the device that used a BaF_2 interfacial layer with that that has a metal fluoride, LiF, used widely as an interfacial layer. The V_{oc} was slightly higher in the device that used BaF_2 (1 nm) than in the device that used LiF (1 nm), which results in a slight increase of PCE from 3.8% (LiF) to 4.0% (BaF_2) (Figure 8).

The BaF_2 layer increased the device lifetime significantly (Figure 9). Device degradation was determined by measuring the device half-life in terms of PCE under continuous simulated solar irradiation at 100 mW cm^{-2}. The device with a 1 nm BaF_2 interfacial layer had a half-life (545 h) that was nine times longer than that of the device without an interfacial layer (60 h) (Figure 9); this difference implies that the cathode interface has a dominant influence on the device lifetime.[15,27,28] <

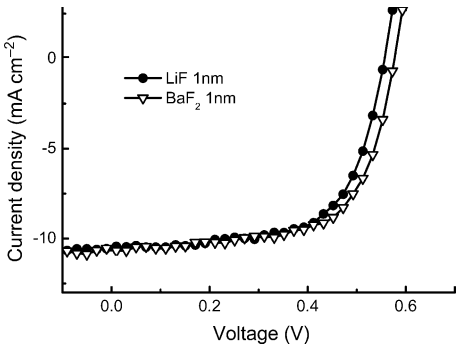

Figure 8. Comparison of the optimized P3HT:PCBM solar cells that have a BaF_2 or LiF interlayer. *J–V* characteristics of the devices with LiF (1 nm) and BaF_2 (1 nm) interlayers under simulated solar AM 1.5 G illumination at an intensity of 100 mW cm^{-2}. P3HT:PCBM films were dried slowly (≈12 min) to maximize the performance.

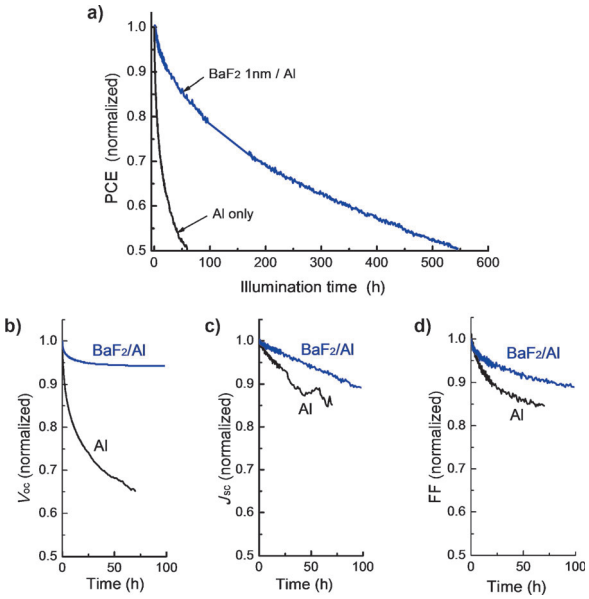

Figure 9. Stability measurement of P3HT:PCBM solar cells kept under continuous simulated solar irradiation at 100 mW cm^{-2}. a) PCEs of the devices that have three different cathode structures over time. Comparison of performance parameters: Changes over time of b) V_{oc}, c) J_{sc}, and d) FF of the continuously illuminated device that has a BaF_2/Al cathode or an Al cathode.

If the device performance parameters of our BaF_2/Al device were compared with those of an Al-only device during the device stability measurement, the device without an interfacial layer was degraded mainly in the performance parameter of V_{oc} under solar irradiation (100 mW cm^{-2} in 25 °C). This means that the BaF_2 interfacial layer plays a critical role to preserve the V_{bi} and V_{oc} of the devices during the photovoltaic operation, which can be attributed to prevention of Al diffusion into the active layer by the metal fluoride interlayer.[28] We also found that the BaF_2 layer blocks the diffusion of Al into the P3HT:PCBM layer (Figure S3).

We collected photoluminescence (PL; Figure 10a) and UV absorption spectra (Figure 10b) from a driven OPV pixel exposed to continuous solar simulated irradiation (100 mW cm^{-2})

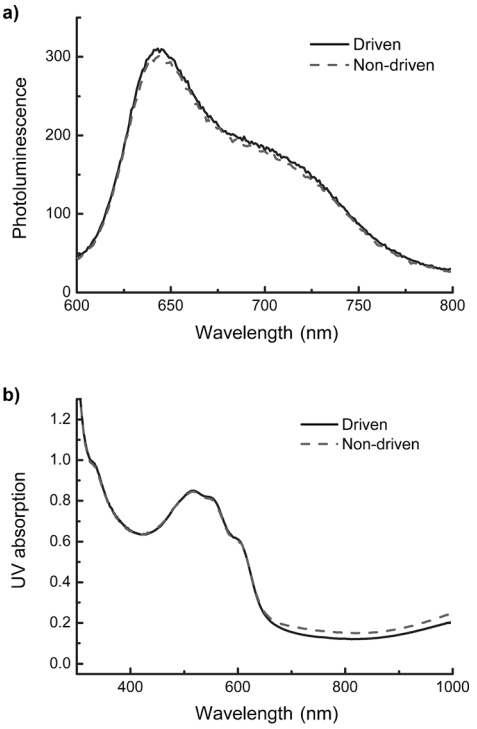

Figure 10. Spectra of driven and undriven OPVs. Driven cell: OPV devices were exposed to continuous simulated solar irradiation at 100 mW cm^{-2} until the PCE was reduced by 50%. Undriven cell: OPV devices were stored under dark conditions for the same period. a) PL and b) UV absorption < spectra.

until the PCE decayed to the half of the initial value and compared them with those of the fresh OPV pixel stored under dark conditions over the same period. To measure the UV absorption spectra of the devices, the cathode layers were carefully detached by using scotch tape. The PL and UV absorption spectra of the illuminated (i.e., driven) pixel were almost identical to those of the unilluminated (i.e., undriven) pixel. These results show clearly that the molecular degradation of P3HT:PCBM is not a major cause of OPV device degradation. Instead of the photodegradation of the organic material, interfacial degradation caused by Al diffusion into the organic layers during device operation is one of the major causes of device degradation.[26,28]

Conclusions

Thin BaF_2 interfacial layers were used as a cathode interlayer to improve the power conversion efficiency (PCE) and device lifetime in organic photovoltaic cells. As a reaction occurred between Al and BaF_2, the released Ba and resultant formation of AlF_3 upon reaction changed the effective cathode work function, the built-in potential, and thus the open-circuit voltage (V_{oc}) of the devices. The BaF_2 interfacial layer follows an island-growth mode so that the V_{oc} strongly depended on the morphological evolution of this layer. This dependence resulted in a gradual increase of the V_{oc} and PCE with BaF_2 layer thickness because of incomplete coverage in the thickness range below the thickness of a single-coverage layer (≈3 nm). However, after the BaF_2 layer thickness exceeded a single-coverage layer, the PCE tended to decrease; this can be explained by an increased series resistance and thus reduced fill factor because of the insulating nature of the thick BaF_2 and space charges accumulated by the insulating layer inside the devices. X-ray photoelectron spectroscopy indicated that the Al deposition on BaF_2 indeed dissociated BaF_2 to form an AlF_3 layer that exists only at the interface between BaF_2 and Al. We also demonstrated that the lifetime of devices with a BaF_2 interfacial layer was significantly longer (approximately nine times) than that of a device without an interfacial layer under continuous simulated solar irradiation (100 mW cm^{-2}); this result indicates the importance of the interfacial layer on the device lifetime.

Experimental Section

Device fabrication

A PEDOT:PSS (CLEVIOS™ PH) dispersion was diluted in isopropyl alcohol (1:1 w/w), spin-coated to give a 35 nm thick hole-extraction layer on top of indium-tin-oxide (ITO)/glass, and baked on a hotplate in air at 200 °C for 10 min. The photoactive layer was composed of a 1:1 mixture of P3HT (regioregularity > 98%, average molecular weight (M_w) ≈25700, RiekeMatals Inc., P200) and PCBM(nano-C Inc.) in anhydrous 1,2-dichlorebenzene (DCB) (Sigma–Aldrich). A P3HT:PCBM:DCB (20 mg/20 mg/1.5 mL) solution was heated at 60 °C fo14 h to achieve good homogeneity. After the PEDOT:PSS/ITO substrates were moved to a N_2-filled glovebox, the P3HT:PCBM solution was spin-on the PEDOT:PSS to give 210 nm thickness, then dried sufficiently slowly (3–12 min) to allow time to enhance the molecular ordering. Then the substrates were baked in a vacuum hotplate at 150 °C for 30 min. The BaF_2 interlayer was thermally evaporated on the P3HT:PCBM film at a deposition rate of 0.1 Å s^{-1} under high vacuum (< 5×10^{-7} Torr), and the Al cathode was deposited sequentially: first, 20 nm thickness at a deposition rate of 1 Å s^{-1} and then 80 nm thickness at 5 Å s^{-1} under high vacuum (< 5×10^{-7} Torr). The photoactive area (0.06 cm^2) was defined by using metallic shadow masks. The devices were encapsulated with a glass lid by using a UV-curable epoxy resin in a N_2-filled glovebox.

Device characterization

The *J–V* characteristics were obtained by using a computer-controlled Keithley 2400 source measurement unit under simulated solar AM 1.5G illumination (100 mW cm^{-2}) generated by using a Xe-lamp-based solar simulator system (Newport 69907, Class AAA, 450 W).

The device stability was measured by using a McSciencePolaronixK3600 Solar Cell Reliability Test System. The J_{sc}, V_{oc}, FF, and PCE were recorded over time under continuous illumination with solar simulated light (air mass 1.5 G, 100 mW cm^{-2}). Photoelectron spectroscopy measurements were conducted by using a modified KRATOS AXIS165 system connected to a home-built organic and metal deposition chamber so that all the film depositions and measurements could be conducted without exposing the samples to ambient pressure. The energy resolution of XPS was approximately1.0 eV. The base pressure of the measurement and the deposition chambers were 1.0×10^{-9} and 1×10^{-8} Torr, respectively. All depositions and measurements were conducted at RT.

Acknowledgements

This work was supported by the National Research Foundation of Korea (NRF) grant funded by the Korean government (MSIP) (NRF-2013R1A2A2A01068753 and NRF-2011-0015172). This work was also supported by a grant from the Center for Advanced Soft Electronics (Code No. 2013M3A6A5073175) under the Global Frontier Research Program of the Ministry of Science, ICT & Future Planning, Korea.

Keywords: aluminum · barium · electron transfer · interfaces · photoelectron spectroscopy

[1] a) L. Chen, Z. Hong, G. Li, Y. Yang, *Adv. Mater.* **2009**, *21*, 1434 – 1449; b) G. Dennler, M. C. Scharber, C. J. Brabec, *Adv. Mater.* **2009**, *21*, 1323 – 1338; c) C. J. Brabec, S. Gowrisanker, J. J. M. Halls, D. Laird, S. Jia, S. P. Williams, *Adv. Mater.* **2010**, *22*, 3839 – 3856; d) M. Helgesen, R. Søndergaard, F. C. Krebs, *J. Mater. Chem.* **2010**, *20*, 36 – 60; e) J. Peet, A. J. Heeger, G. C. Bazan, *Acc. Chem. Res.* **2009**, *42*, 1700 – 1708; f) J. Peet, M. L. Senatore, A. J. Heeger, G. C. Bazan, *Adv. Mater.* **2009**, *21*, 1521 – 1527; g) H. B. Yang, Q. L. Song, C. M. Li, Z. S. Lu, *Energy Environ. Sci.* **2008**, *1*, 389 – 394; h) T. Ameri, G. Dennler, C. Lungenschmied, C. J. Brabec, *Energy Environ. Sci.* **2009**, *2*, 347 – 363; i) M. K. Siddiki, J. Li, D. Galipeau, Q. Qiao, *Energy Environ. Sci.* **2010**, *3*, 867.

[2] a) C. J. Brabec, N. S. Sariciftci, J. C. Hummelen, *Adv. Funct. Mater.* **2001**, *11*, 15 – 26; b) W. Ma, C. Yang, X. Gong, K. Lee, A. J. Heeger, *Adv. Funct. Mater.* **2005**, *15*, 1617 – 1622; c) P. Schilinsky, U. Asawapirom, U. Scherf, M. Biele, C. J. Brabec, *Chem. Mater.* **2005**, *17*, 2175 – 2180; d) C. Yang, J. G. Hu, A. J. Heeger, *J. Am. Chem. Soc.* **2006**, *128*, 12007 – 12013; e) J. Xue, B. P. Rand, S. Uchida, S. R. Forrest, *J. Appl. Phys.* **2005**, *98*, 124903; f) R. J. Kline, M. D. McGehee, M. F. Toney, *Nat. Mater.* **2006**, *5*, 222 – 228; g) X. Yang, J. Loos, S. C. Veenstra, W. J. H. Verhees, M. M. Wienk, J. M. Kroon, M. A. J. Michels, R. A. J. Janssen, *Nano Lett.* **2005**, *5*, 579 – 583; h) F. Zhang, W. Mammo, L. M. Andersson, S. Admassie, M. R. Andersson, O. Inganäs, *Adv. Mater.* **2006**, *18*, 2169 – 2173; i) W.-Y. Wong, X.-Z. Wang, Z. He, A. B. Djurisic, C.-T. Yip, K.-Y. Cheung, H. Wang, C. S. K. Mak, W.-K. Chan, *Nat. Mater.* **2007**, *6*, 521 – 257; j) M. Morana, M. Wegscheider, A. Bonanni, N. Kopidakis, S. Shaheen, M. Scharber, Z. Zhu, D. Waller, R. Gaudiana, C. J. Brabec, *Adv. Funct. Mater.* **2008**, *18*, 1757 – 1766; k) J. Gilot, M. M. Wienk, R. A. J. Janssen, *Nat. Mater.* **2007**, *6*, 704; l) T. Erb, U. Zhokhavets, G. Gobsch, S. Raleva, B. Stühn, P. Schilinsky, C. Waldauf, C. J. Brabec, *Adv. Funct. Mater.* **2005**, *15*, 1193 – 1196; m) M. H. Yun, G.-H. Kim, C. Yang, J. Y. Kim, *J. Mater. Chem.* **2010**, *20*, 7710 – 7714.

[3] a) T.-W. Lee, K.-G. Lim, D.-H. Kim, *Electron. Mater. Lett.* **2010**, *6*, 41 – 50; b) J. H. Park, T.-W. Lee, B.-D. Chin, D. H. Wang, O. O. Park, *Macromol. Rapid Commun.* **2010**, *31*, 2095; c) L.-M. Chen, Z. Xu, Z. Hong, Y. Yang, *J. Mater. Chem.* **2010**, *20*, 2575 – 2598; d) H.-L. Yip, A. K.-Y. Jen, *Energy Environ. Sci.* **2012**, *5*, 5994 – 6011; e) M.-R. Choi, T.-H. Han, K.-G. Lim, S.-H. Woo, D. H. Huh, T.-W. Lee, *Angew. Chem. Int. Ed.* **2011**, *50*, 6274 – 6277; *Angew. Chem.* **2011**, *123*, 6398 – 6401.

[4] S. H. Park, A. Roy, S. Beaupre, S. Cho, N. Coates, J. S. Moon, D. Moses, M. Leclerc, K. Lee, A. J. Heeger, *Nat. Photonics* **2009**, *3*, 297 – 303.

[5] H.-Y. Chen, J. Hou, S. Zhang, Y. Liang, G. Yang, Y. Yang, L. Yu, Y. Wu, G. Li, *Nat. Photonics* **2009**, *3*, 649 – 653.

[6] M. O. Reese, M. S. White, G. Rumbles, D. S. Ginley, S. E. Shaheen, *Appl. Phys. Lett.* **2008**, *92*, 053307.

[7] V. D. Mihailetchi, P. W. M. Blom, J. C. Hummelen, M. T. Rispens, *J. Appl. Phys.* **2003**, *94*, 6849 – 6854.

[8] X. Jiang, H. Xu, L. Yang, M. Shi, M. Wang, H. Chen, *Sol. Energy Mater. Sol. Cells* **2009**, *93*, 650 – 653.

[9] S. K. M. Jönsson, E. Carlegrim, F. Zhang, W. R. Salanck, M. Fahlman, *Jpn. J. Appl. Phys.* **2005**, *44*, 3695 – 3701.

[10] C. J. Brabec, S. E. Shaheen, C. Winder, N. S. Sariciftci, *Appl. Phys. Lett.* **2002**, *80*, 1288 – 1290.

[11] S. E. Shaheen, G. E. Jabbour, M. M. Morrell, Y. Kawabe, B. Kippelen, N. Peyghambarian, M.-F. Nabor, R. Schlaf, E. A. Mash, N. R. Armstrong, *J. Appl. Phys.* **1998**, *84*, 2324 – 2327.

[12] G. Li, V. Shrotriya, Y. Yao, Y. Yang, *J. Appl. Phys.* **2005**, *98*, 043704.

[13] G. Li, V. Shrotriya, J. Huang, Y. Yao, T. Moriarty, K. Emery, Y. Yang, *Nat. Mater.* **2005**, *4*, 864 – 868.

[14] T.-W. Lee, M. G. Kim, S. H. Park, S. Y. Kim, O. Kwon, T. Noh, J. J. Park, T. L. Choi, J. H. Park, B. D. Chin, *Adv. Funct. Mater.* **2009**, *19*, 1863 – 1868.

[15] X. Yang, Y. Mo, W. Yang, G. Yu, Y. Cao, *Appl. Phys. Lett.* **2001**, *79*, 563 – 565.

[16] T. M. Brown, R. H. Friend, I. S. Millard, D. J. Lacey, T. Butler, J. H. Burroughes, F. Cacialli, *J. Appl. Phys.* **2003**, *93*, 6159 – 6172.

[17] G. G. Malliaras, J. R. Salem, P. J. Brock, J. C. Scott, *J. Appl. Phys.* **1998**, *84*, 1583 – 1587.

[18] a) T.-W. Lee, J. Zaumseil, S. H. Kim, J. W. P. Hsu, *Adv. Mater.* **2004**, *16*, 2040 – 2045; b) T.-W. Lee, O. O. Park, L.-M. Do, T. Zyung, T. Ahn, H.-K. Shim, *J. Appl. Phys.* **2001**, *90*, 2128 – 2134.

[19] R. W. Zehner, B. F. Parsons, R. P. Hsung, L. R. Sita, *Langmuir* **1999**, *15*, 1121 – 1127.

[20] a) S. L. M. van Mensfoort, R. Coehoorn, *Phys. Rev. Lett.* **2008**, *100*, 086802; b) K.-G. Lim, M.-R. Choi, H.-B. Kim, J. H. Park, T.-W. Lee, *J. Mater. Chem.* **2012**, *22*, 25148 – 25153.

[21] J. Lee, Y. Park, D. Y. Kim, H. Y. Chu, H. Lee, L.-M. Do, *Appl. Phys. Lett.* **2003**, *82*, 173 – 175.

[22] Y. K. Kim, J. W. Kim, Y. Park, *Appl. Phys. Lett.* **2009**, *94*, 063305.

[23] a) G. E. Jabbour, Y. Kawabe, S. E. Shaheen, J. F. Wang, M. M. Morrell, *Appl. Phys. Lett.* **1997**, *71*, 1762 – 1764; b) Q. T. Le, L. Yan, Y. Gao, M. G. Mason, D. J. Giesen, *J. Appl. Phys.* **2000**, *87*, 375 – 379; c) J. Lee, J. S. Lim, H. J. Shin, Y. Park, *Appl. Phys. Lett.* **2007**, *91*, 261902.

[24] O. Bose, E. Kemnitz, A. Lippitz, W. E. S. Unger, *Fresenius J. Anal. Chem.* **1997**, *358*, 175 – 179.

[25] R. Long, J. Luo, M. Chen, H. Wan, *Appl. Catal. A* **1997**, *159*, 171 – 185.

[26] S. T. Lee, Z. Q. Gao, L. S. Hung, *Appl. Phys. Lett.* **1999**, *75*, 1404 – 1406.

[27] a) R. Rösch, D. M. Tanenbaum, M. Jørgensen, M. Seeland, M. Bärenklau, M. Hermenau, E. Voroshazi, M. T. Lloyd, Y. Galagan, B. Zimmermann, U. Würfel, M. Hösel, H. F. Dam, S. A. Gevorgyan, S. Kudret, W. Maes, L. Lutsen, D. Vanderzande, R. Andriessen, G. Teran-Escobar, M. Lira-Cantu, A. Rivaton, G. Y. Uzunoglu, D. Germack, B. Andreasen, M. V. Madsen, K. Norrman, H. Hoppe, F. C. Krebs, *Energy Environ. Sci.* **2012**, *5*, 6521 – 6540; b) N. Grossiord, J. M. Kroon, R. Andriessen, P. W. M. Blom, *Org. Electron.* **2012**, *13*, 432 – 455; c) M. Jørgensen, K. Norrman, F. C. Krebs, *Solar Energy Mater. Solar Cells* **2008**, *92*, 686 – 714; d) M. Wang, Q. Tang, J. An, F. Xie, J. Chen, S. Zheng, K. Y. Wong, Q. Miao, J. Xu, *ACS Appl. Mater. Interfaces* **2010**, *2*, 2699 – 2702; e) K. Kawano, C. Adachi, *Appl. Phys. Lett.* **2010**, *96*, 053307; f) Y. Cao, G. Yu, I. D. Parker, A. J. Heeger, *J. Appl. Phys.* **2000**, *88*, 3618 – 3623.

[28] a) M. D. Wang, F. Y. Xie, W. G. Xie, S. Z. Zheng, N. Ke, J. Chen, N. Zhao, J. B. Xu, *Appl. Phys. Lett.* **2011**, *98*, 183304; b) Y. Suh, N. Lu, S. H. Lee, W. S. Chung, K. Kim, B. S. Kim, M. J. Ko, M. J. Kim, *ACS Appl. Mater. Interfaces* **2012**, *4*, 5118 – 5124; c) W. Song, S. K. So, J. Moulder, Y. Qiu, Y. Zhu, L. Cao, *Surf. Interface Anal.* **2001**, *32*, 70 – 73; d) W. Song, Z. Li, S. K. So, Y. Qiu, Y. Zhu, L. Cao, *Surf. Interface Anal.* **2001**, *32*, 102 – 105; e) Y. Hirose, A. Kahn, V. Aristov, P. Soukiassian, V. Bulovic, S. R. Forrest, *Phys. Rev. B* **1996**, *54*, 13748 – 13758; f) Y. Hirose, A. Kahn, V. Aristov, P. Soukiassian, *Appl. Phys. Lett.* **1996**, *68*, 217 – 219.

Received: October 26, 2013
Published online on February 25, 2014